Physics – Uspekhi **67** (1) 80 – 90 (2024)

METHODOLOGICAL NOTES PACS numbers: **05.40.– a**, **91.30.– f**, **92.60.– e**

A N Kolmogorov's 1934 paper is the basis for explaining the statistics of natural phenomena of the macrocosm

G S Golitsyn

DOI: https://doi.org/10.3367/UFNe.2023.05.039355

Contents

Abstract. The 1934 paper by A N Kolmogorov [1], "Random Motions," hereinafter ANK34, uses a Fokker–Planck-type equation for a 6-dimensional vector with a total rather than a partial derivative with respect to time, and with a Laplacian in the space of velocities. The diffusion coefficient in this case is ε, the rate of energy generation/dissipation. The equation is obtained by specifying the accelerations of the particles of the ensemble by Markov processes, i.e., random processes δ-correlated in time and with each other. The fundamental solution of this equation was already indicated in [1] and was used by A M Obukhov [2] in 1958 to describe a turbulent flow in the inertial interval [3]. It was only recently [4, 5] noticed that the Fokker–Planck-type equation written by Kolmogorov in [1] contains a description of the statistics of other random natural processes, earthquakes, sea waves, and others [5]. This equation, by a change of variables with scales for velocities and for coordinates, is reduced to a self-similar form that does not explicitly contain the diffusion coefficient [6]. Numerical calculations confirm the presence of such scales in systems with the number N of events, in ensembles starting from $N = 10$. For $N = 100$, these scales almost exactly coincide with the ANK34 theory. This theory, in principle, containing the results of 1941, paved the way for more complex random systems with enough parameters to form an external similarity parameter. This leads to a change in the characteristics of a random process, for example, to a change in the slope of the time spectrum, as in the case of earthquakes and in a number of other processes (sea waves, cosmic ray energy spectrum, inundation zones during floods, etc.). A review of specific random processes studied experimentally provides a methodology for how to proceed when comparing experimental data with the ANK34 theory. Thus, empirical data illustrate the validity of the fundamental laws of probability theory. The article is an abridged version of the author's monograph [5], where for the first time the ideas of ANK34 were used to explain in a probabilistic sense many experimental patterns that have been considered by pure empiricism for decades.

Keywords: random motions, Fokker–Planck–Kolmogorov equation, second moments of probability distribution for coordinates and velocities, theory of similarity and dimensions, statistical laws of nature

90th anniversary of the publication of A N Kolmogorov's paper, "Random motions" [1]

1. General information

In 1934, Andrey Nikolaevich Kolmogorov published a two-page article entitled "Zufällige Bewegungen" ("Random motions"), which provided a background for the physical and mathematical explanation of the statistical laws of nature [1] (ANK34). An equation from ANK34 has the form

$$\frac{\partial p(u_i, x_i, t)}{\partial t} + u_k \frac{\partial p(u_i, x_i, t)}{\partial x_k} = D \frac{\partial^2 p(u_i, x_i, t)}{\partial u_k^2} \qquad (1)$$

and differs from the conventional Fokker–Planck (FP) equation by the full (substantial) time derivative on the left-hand side of the probability density function of the six-dimensional random vector $\mathbf{A} = (u_i, x_i)$ instead of $\partial p(t, x_i)/\partial t$ $(i, k = 1, 2, 3)$, with summation assumed over the repeating indices. The diffusion coefficient in the velocity space has the dimension of the velocity squared over time, i.e., $[D] = L^2 T^{-3}$. A M Obukhov [2] was the first to use this

G S Golitsyn
A M Obukhov Institute of Atmospheric Physics,
Russian Academy of Sciences,
Pyzhevskii per. 3, 109017 Moscow, Russian Federation
E-mail: gsg@ifaran.ru

Received 16 February 2023
Uspekhi Fizicheskikh Nauk **194** (1) 86 – 96 (2024)
Translated by S D Danilov

equation, notably for the description of turbulence. He also showed that the diffusion coefficient D for the inertial range of turbulence is equal to the rate of generation/dissipation of kinetic energy. He foresaw that this equation could also be applied to other processes of a statistical nature. The conventional FP equation describes random *walk*, and (1) describes random *motions*.

A M Obukhov showed in [2, 3] that the probability density $p(t, u_i, x_i)$ has three second moments in the inertial range of turbulent flows which grow with time. With angular brackets denoting statistical averaging,

$$\langle u_i^2(t)\rangle = \varepsilon t\,, \tag{2}$$

$$\langle x_i^2(t)\rangle = \varepsilon t^3 = r^2\,, \tag{3}$$

$$\langle u_i x_i\rangle = \varepsilon t^2 = K\,. \tag{4}$$

Expressing time from (3),

$$t = \left(\frac{r^2}{\varepsilon}\right)^{1/3} \tag{5}$$

and inserting it into (2) and (4), we obtain the Kolmogorov law for the velocity structure function for zero (or small) initial value,

$$u^2(r) = \varepsilon t = (\varepsilon r)^{2/3}\,, \tag{6}$$

$$\langle u_i x_i\rangle = K = \varepsilon^{1/3} r^{4/3}\,, \tag{7}$$

where K is the kinematic mixing coefficient.

In the last two formulas, we have purposely not mentioned the universal dimensionless constants which should be determined by making a comparison with experiments. Such experiments are carried out under different conditions (for example, under different boundary conditions). For reference, one such constant in formula (6) is $C_6 \approx 1.6$, and one gets $C_7 \approx 0.18$ in formula (7) [3]. Formula (7) is the Richardson–Obukhov law of turbulent diffusion.

Let us consider the second moments (2)–(4) in some detail. Equation (1) can be reduced to a fully self-similar form by the variable transformation $u_i(t) = (\varepsilon t)^{1/2} v_i$, $x_i = (\varepsilon t^3)^{1/2} y_i$, in which case the dimensionless variables v_i, y_i will eliminate the diffusion coefficient D from (1).

The fundamental solution of equation (1) can be written as

$$p(t, u_i, x_i) = \left(\frac{\sqrt{3}}{2\pi D t}\right)^3 \exp\left[-\left(\frac{u_i^2}{Dt} - \frac{3u_i x_i}{Dt^2} + \frac{3x_i^2}{Dt^3}\right)\right]. \tag{8}$$

This expression was first presented in [3], where it is formula (24.56). It shows in an obvious way that our nondimensionalization maximizes the probability in (8) in a certain sense.

When A M Obukhov presented these results at the International Symposium on Pollution of the Atmosphere in 1958, G Batchelor asked him what new element is given by such an approach as compared with the use of the similarity theory and dimensional considerations. The equation from ANK34 gives a description of random processes as they evolve with time, but formula (5) connects the temporal and spatial characteristics of the processes under consideration, and therefore this formula can be considered a dispersion relation for $\omega = 2\pi/t$ and $k = 2\pi/r$,

$$\omega = (2\pi\varepsilon)^{1/3} k^{2/3}\,, \tag{9}$$

whose nonlinearity introduces major analytical complications. The consideration of dimension and similarity, which has become an exact science in its own right [7], is another method of process analysis; it complements ANK34 and extends its scope. When considering the full set of parameters of a phenomenon, one can form dimensionless similarity parameters that can be included in the dimensionless coefficients that appear when the ANK formulas are compared with experimental data. An essential new concept for such studies is the concept of 'intermediate asymptotic forms' [8, 9], introduced by G I Barenblatt and Ya B Zel'dovich. The applicability limits of this asymptotic form are established by comparison with experiments based on the analysis of the similarity numbers of the phenomena under study.

Analytical formulas of the probability theory are derived under the assumption that there is an infinite ensemble of events to be considered. In practice, the number of events is always finite, sometimes only in the order of ten. Therefore, the effect of the finite ensemble size N on formulas (2)–(4) needs to be investigated. To this end, numerical simulations were carried out in [6]. Equations

$$\dot{u}_i = a_i\,, \quad \dot{x}_i = u_i\,, \tag{10}$$

where $i = 1, 2, \ldots, N$ is the total number of pairs of such equations, and a_i is the acceleration of a single particle without interaction with other particles, have been solved numerically. For simplicity, equations (10) were solved en masse for a one-dimensional case. However, the main relations apply to two- and three-dimensional cases. The accelerations a_i were given by different types of distributions. The choice of the distribution functions and time step has no significant effect on the second moments of the velocities and displacements of the Lagrangian particles. The results of such simulations are shown in Fig. 1. It can be seen that, for the total number of particles $N = 10$, the second moment is proportional to time, despite apparent fluctuations. The second moment of the displacements follows the dependence $\langle x^2(t)\rangle \sim t^3$ practically exactly. The distances between particles are obtained by integrating the velocities, which is equivalent to smoothing.

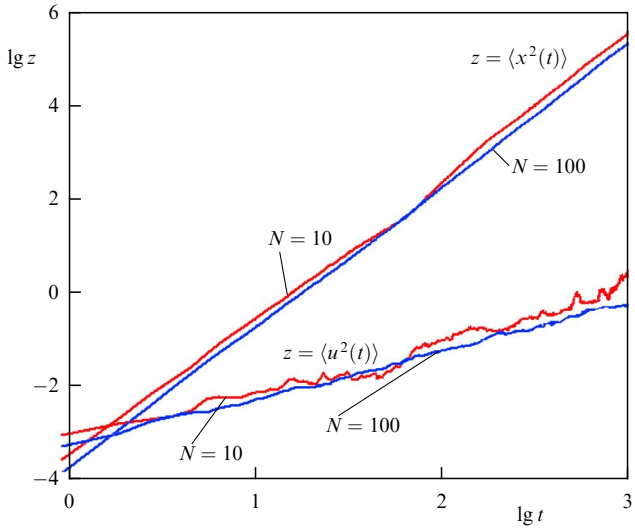

Figure 1. Second moments of the probability density function for velocities $\langle u^2(t)\rangle$ and distances between particles $\langle x^2(t)\rangle \sim t^3$.

We assume that the Lagrangian results are also applicable in the Eulerian description, based on the fact that, under this assumption, one can well describe real experimental data, which was tested in [6]. The moments (2) and (3) will be considered to be structure functions with zero or small initial data; the same relationships hold for the individual components of 6-dimensional vector $u_i x_i$. We write (3) for the vertical coordinate $\langle h^2(t)\rangle \approx \varepsilon t^3$. If h is the height of the peak of sea waves, and t the peak period, then we have the famous relationship between the peak height and period, discovered in 1978 [10]. This relationship was then found with unusual accuracy, with the correlation coefficient $r > 0.99$ (see Section 4 for an explanation). The structure function (3) implies [3] the frequency spectrum εk^{-4}, which was shown by the same author [11] in 1973.

Expression (2) for the mean square velocity can be considered to give the energy of a particle per unit mass. Such a formula was first proposed in 1944 by L D Landau in the first edition of *Mekhanika Sploshnykh Sred* (*Mechanics of Continuous Media*), which contains the expression $u^2 \approx \varepsilon t$. These moments immediately give a description of cumulative probability distributions, sometimes called integral distributions, which have the dimension of inverse time, i.e., frequency,

$$N(\geqslant E) \approx \frac{\varepsilon}{E} \tag{11}$$

for the events associated with energy, and for spatial processes, formula (3) allows us to write

$$N(\geqslant S) \sim \left(\frac{\varepsilon}{S}\right)^{1/3}, \tag{12}$$

which gives the distribution for lithospheric plates [13] that remained mysterious for many years. The same distribution is found in [5] for the masses of the nearest spiral galaxies, assuming that their mass is proportional to their surface area.

Another observation about second moments immediately solves the problem posed by Sir James Lighthill in 1995. In the last decade of the 20th century, the UN proclaimed the International Decade for Natural Disaster Reduction, and Sir Lighthill, a fluid dynamicist and member of many academies, including our own, became the head of the Scientific Steering Committee. He said that we did not understand how the kinetic energy of a tropical hurricane could reach the energy level of the explosion of many thousands of megaton bombs. The answer is to multiply the product of the first two moments by the mass density of the atmospheric column $M = 10^4\ \mathrm{kg\,m^{-2}}$, which these hurricanes penetrate at up to 15–18 km. The energy is generated by the concentration of angular momentum, driven by convection. The buoyancy flux in this case is of the order of $b = \varepsilon = \alpha g f/\rho c_p \approx 0.03\ \mathrm{m^2\ s^{-3}}$, and for the energy is the equation

$$E = Mb^2 l_C^{-4}, \tag{13}$$

where $l_C = (4\pi/T)\sin\theta$ is the Coriolis parameter, which is inversely proportional to the rotation period, and θ is the latitude. For $l_C = 0.5 \times 10^{-4}$ at the latitude of 20°, we find [5, 15, 16] $E \approx 10^{19}$ J. This number is backed by thousands of papers. The explosion energy for 1 Mt of TNT $= 1.6 \times 10^{15}$ J. Formula (13) was obtained earlier in 1997 by the methods of similarity theory and dimensional analysis. Overall, this earlier approach and ANK34 allow the subject of the studies to be considered from different angles, supporting each other.

We will now turn to the consideration of individual processes, uncovering their specific and general features. In comparison with experiments, when the quantities with the same dimensions are considered, dimensionless numerical multipliers appear, which in turn may depend on other similarity parameters if there is a sufficient number of dimensional governing parameters in the system [7].

2. Earthquakes

An overwhelming number of earthquakes (EQs), more than 90%, occur near the boundaries of lithospheric plates. Convection in the mantle with velocities of several cm $\mathrm{yr^{-1}}$ is inhomogeneous in space and time. By entraining the plates, convection creates stresses at their boundaries, which are released by a rupture and an EQ in Earth's crust. In the early 1940s, an empirical law was established for the occurrence of EQs as a function of their magnitude [17, 18], which became known as the Gutenberg–Richter (GR) law,

$$\lg N(\geqslant m) = a - bm, \tag{14}$$

where $N(\geqslant m)$ is the cumulative number of EQs of magnitude $\geqslant m$ during the time interval studied; a is a constant that depends on the choice of measurement units, the time interval, and also the place of observation; and $b \approx 1$. The magnitude m is related to the logarithm of the EQ energy and is estimated by the amplitude of the surface or volume seismic waves [18].

The analysis of seismograms allows one to estimate the parameters of the fault: length L, area S, development time τ, and mean displacement of the crustal blocks along the fault u, and also to calculate the seismic moment, the measure of EQ energy in the form (see [18])

$$M = \mu S u, \tag{15}$$

where μ is the crustal shear modulus. There is an approximate relationship between the values of magnitude and seismic moment that is supported by some theoretical considerations and observational statistics [17, 18],

$$m = \frac{2}{3}\lg M - 6, \tag{16}$$

where the quantity M is measured in SI units, i.e., [N m]. The quantity M is the torque of the forces acting in the system, i.e., it is the absolute value of the tensor (see Kasahara [18]). Dimensionally, the moment is equal to the energy. In terms of the moment, the GR law (14) is written with the exponent $b' \approx 2/3$. From this and from (14), it then follows that

$$N(\geqslant M) \sim M^{-2/3}.$$

Kanamori and Anderson (see [18]), based on a simple model for rupture and fault dynamics and also on the postulated scaling, assumed that the drop in stresses $\Delta\sigma$ in the crust (accompanying an EQ) is approximately constant and found that the fault area $S \propto M^{2/3}$. This is true [7] for EQs with $m \geqslant 6$. This gives another interpretation of the magnitude [17, 18]

$$m = \lg\left(\frac{S}{S_0}\right), \tag{17}$$

where $S_0 \approx 100\ \mathrm{m^2} = 0.01$ ha $= 1$ are.

A special test has shown that the drop in stresses (see [5]) in the crust is about 4.5 MPa for a change in the module of the moment tensor of 5–6 orders of magnitude. Analysis of global EQ catalogs has shown that there is a value $M_{cr} \approx 1.6 \times 10^{20}$ N m around which the quantity b in (14) varies from 1 to 1.5. This is certainly observed for the EQ near mid-ocean ridges, where the magma spreads outward at the rate of 3 km^3 yr^{-1} and solidifies in the crust, and where the crust is thin. To analyze the EQ process, we first use the similarity theory [17].

We take the shear modulus $\mu = (3-7) \times 10^{10}$ N m^{-2}, the density $\rho = 3 \times 10^5$ kg m^{-3}, and the stress drop $\Delta\sigma = 4.5 \times 10^6$ N m^{-2} as the material constants of the crust [18]. The origin and the measure of the power of all geodynamical processes is the geothermal flux $F \approx 4.5 \times 10^{13}$ W with an geothermal flux density of 86 mW m^{-2} [19]. The global data for EQs also reveal the thickness of the plates h. We have four parameters with three dimensions. One can form the length and time scales [17] that characterize an individual EQ,

$$L = \left(\frac{M}{\Delta\sigma}\right)^{1/3}, \qquad T = \frac{M}{F}.$$

In the 20th century, the strongest EQ, with $m = 9.5$, i.e., $\lg M = 20$, occurred in Chile in 1960. The four external system parameters lead to one dimensionless similarity parameter

$$\Pi = \frac{L}{h} = \frac{M^{1/3}}{\Delta\sigma^{1/3} h}. \tag{18}$$

Based on the dimensional consideration, we can write the number of events with the dimension of frequency

$$N(\geqslant M) = \frac{F}{M} f(\Pi), \tag{19}$$

where $f(\Pi)$ is some function Π of the similarity parameter which has to be determined from observations. According to global catalogs, $\Pi \geqslant 1$ near the mid-ocean ridges, and so we can assume that $f(\Pi) \to$ const. For $\Pi < 1$, this function can be expanded in the Maclaurin series, which should begin from a linear term (no EQ if there is no excitation). Then, $f(\Pi) = c_1\Pi = c_1 M^{-1/3}\Delta\sigma^{-1/3}/h$. Processing the global catalogs [5, 20] gave the value for the constant $c_1 \approx 0.35$. For $\Pi > 1$, it is also found that $c_1 \approx 0.34 \pm 0.02$ for $b \approx 2/3$. Note that, for $5 < m < 7.5$ in [21], it was found that $b = 0.65 \pm 0.02$. So, if the EQ is inside the crust, then $b \approx 2/3$, and if it goes outside the crust, then $\lg N(\geqslant M) \sim M^{-1}$. EQs with $\Pi > 1$ will occur less frequently than for $\Pi < 1$ when $\lg N(\geqslant M) \sim M^{-2/3}$.

Induced EQs are known to occur after the construction of large water reservoirs or to accompany large-scale gas and oil extraction [22]. In these cases, there are changes in the internal pressure in the system — the quantity $\mathrm{d}p/\mathrm{d}z = -\rho g$. These changes lead to a violation of isostasy, i.e., to the appearance of new stresses and modifications of old stresses in the crust [5, 22, 23]. These EQs are satisfactorily described by the Gutenberg–Richter laws. The spectra of microseisms (Fig. 2) in the two frequency ranges from 1 to 0.1 Hz and from 10^{-2} to 5×10^{-4} Hz behave as $\omega^{-4} \sim T^4$, in accordance with the second moment (3). The first interval reflects the breaking of sea waves with such a spectrum on the coast, and the second corresponds to periods in the minute range due to the combination of numerous random factors inside and outside Earth's crust, in agreement with ANK34.

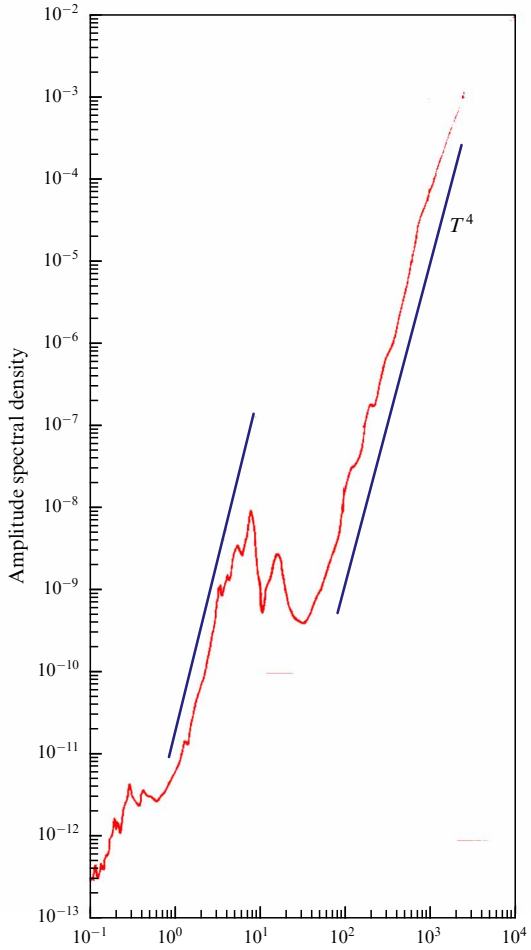

Figure 2. Spectra of microseisms from [5].

Starquakes observed in our Galaxy are also distributed close to the Gutenberg–Richter laws, i.e., under appropriate conditions, these laws apply everywhere [5, 24, 25].

3. Energy spectrum of cosmic rays

The theoretical derivation of this spectrum has been awaited for more than half a century, and the mechanism by which particles of cosmic rays (CRs) are accelerated up to ultra-relativistic energies of 10^{12} GeV was not clear either. In monograph [26], which is still useful in many respects, it is stated that the full explanation of CRs and their spectrum may possibly require some new physics. Already in 1949, Enrico Fermi formulated a hypothesis that acceleration could take place at the inhomogeneities of the galactic magnetic field. However, it was not until 2001 that M Mal'kov [27], the former doctoral student of R Z Sagdeev, explained that the acceleration occurs at the fronts of collisionless shock waves. In 2014, the results of the Russian–European experiment PAMELA were published [28], in which five years of measurements aboard the Resurs-5 spacecraft operating since 2003 showed the power-law character of the spectrum with the exponent $n = 2.67 \pm 0.02$. Figure 3 shows the spectrum based on data from terrestrial measurements [26] with the exponent 2.7 or in the integral (cumulative) form with $n = 1.7$, which is close to 5/3.

In our Galaxy, supernovae explode 2–3 times per century, producing CRs, magnetic fields, turbulence in the interstellar

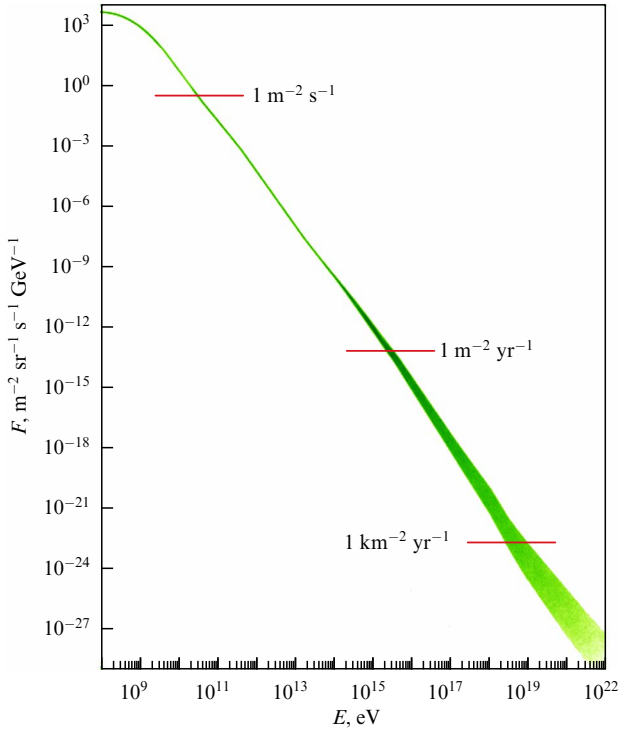

Figure 3. Cosmic ray energy spectrum, Wikipedia.

gas, and shock waves. The experimental determination of the CR spectrum has its own specificity: it is the number of particles detected in a given energy interval per unit time and per *unit area*. This corresponds to an energy supply to the Galaxy with a radius of 50 thousand light years and disk thickness of 200 pc $= 6 \times 10^{18}$ m. The energy of a supernova explosion is $10^{42} - 10^{43}$ J, i.e., the average power entering the system is $G \approx 2 \times 10^{33}$ W, and part of it feeds the acceleration of CRs. Reference [26] gives an estimate for the volume density of the CR energy $w_0 \approx 0.5$ eV cm$^{-3} \approx 10^{-13}$ J m^{-3}. The full energy of the CR particles in the Galaxy is $W \approx 10^{48}$ J. The estimated particle time will be $\tau = W/G = 5 \times 10^{14}$ s $= 1.6 \times 10^7$ yr, while the Galaxy's age is on the order of 10^{10} years, and it has seen about a thousand particle generations. These particles are brought into rotation by the galactic magnetic field with an average amplitude $H \approx 5 \times 10^{-6}$ G [26]. The energy density in this field is about $H^2/8\pi \approx 10^{-13}$ J m^{-3}, i.e., the same as the energy of CRs, and during their lifetime the particles are accelerated many times in random shock waves propagating in the interstellar gas after supernova explosions.

It has been mentioned that the specificity of CRs lies in the measurements per unit area. This quantity can only be obtained from the volume density of the rays. As for a gas, we will assume that this density is $w_0 \sim nE$ (in a gas $E = kT$), where n is the concentration with the dimension cm^{-3}. Then, the quantity with the dimension of area S is estimated as $(w_0/E)^{2/3}$. The concentration over energy [26]

$$n(\geqslant E) = \int_E^\infty n(E)\,\mathrm{d}E = \frac{4\pi}{c}\int_E^\infty I(E)\,\mathrm{d}E = \frac{4\pi}{c}\,I(\geqslant E) \qquad (20)$$

is the quantity proportional to the integral spectrum, and c is the speed of light. Further, it is easier to find the integral spectrum based on dimensional considerations, $I(\geqslant E) = S^{-1}T^{-1}$, $w_0 = ES^{-3/2}$, $G = ET^{-1}$, $[E] = E$; here, we use the dimension of energy instead of mass, and taking the dimension of time from G/E and the area from $(w_0/E)^{2/3}$, we obtain

$$I(\geqslant E) \sim c_1 \frac{G}{E}\left(\frac{w_0}{E}\right)^{2/3} \sim E^{-5/3}\,. \qquad (21)$$

The spectrum after the bend is already defined by particles that are not confined by the magnetic field, i.e., for such particles, the generator is the spectrum given by (21). Repeating the same procedure as for the derivation of (21), we find [29]

$$I(\geqslant E) = C_2 c^{-2/3} G^{5/3} w_0^{4/9} E^{-19/9} \sim E^{-19/9}\,, \qquad (22)$$

while in [26] the spectral index is estimated to be 2.1, and in [28] there were no measurements in this spectral range. We have $19/9 = 2 + 1/9$, i.e., the difference is $1/90$.

What is the relation with ANK34? The integral spectrum $I(\geqslant E)$ is inversely proportional to time, and here lies its connection to the first moment (2), but it is also inversely proportional to the unit of area over which the measurements are made. And this peculiarity of the measurement procedure is the new element, not in physics, but in the *definition* of the spectrum, which causes the appearance of thirds in the spectral exponent.

4. Sea wind waves

Waves on the sea surface are one of the most fascinating natural phenomena. And they are the direct manifestation of ANK34, although this was only discovered in 1978 [10, 11]: Toba found that the mean peak height h is proportional to the power of its period as $T^{3/2}$. This dependence taken to the power of two is the third invariant of ANK34: $h^2 \sim T^3$! Initially, many researchers did not understand the origin of this relationship, until the derivation and the experimental test of the frequency spectrum for sea waves [11], $S_h(\omega) \sim \varepsilon\omega^{-4}$, which leads to the Toba relationship after integration. But now this spectrum is the consequence of the third invariant $\langle x_i^2(t)\rangle = \varepsilon t^3$. If this is considered a structure function [3], its spectrum is exactly $\varepsilon\omega^{-4}$!

In fact, two similarity parameters for wind waves related to wave conditions were established a long time ago, and their relevance was already noticed by seafarers in ancient times. They are the age of sea waves [31, 32]

$$\Omega = \frac{U}{c_\varphi}\,,$$

where U is the wind speed, routinely taken at 10 m above sea level, and c_φ is the phase speed of the main peak. Over deep water, the dispersion relation is $\omega^2 = kg$ and, in this case, $c_\varphi = \omega(k)/k = (g/k)^{1/2}$.

The second similarity parameter is the wave fetch, which is related to the distance x to the windward shore, $F = gx/U^2$. We note that the product $\Omega F = \omega_p x/U = \omega_p T$, where T is the time the wind acts on the waves. It was noticed long ago that young waves are steeper than well-developed waves, which are close breaking. Systematic theoretical studies of sea waves were initiated about 60 years ago by K Hasselmann, who derived kinetic equations for the energy of sea waves and organized experimental studies (he was awarded the 2021 Nobel Prize in Physics). Since then, studies of wave evolution

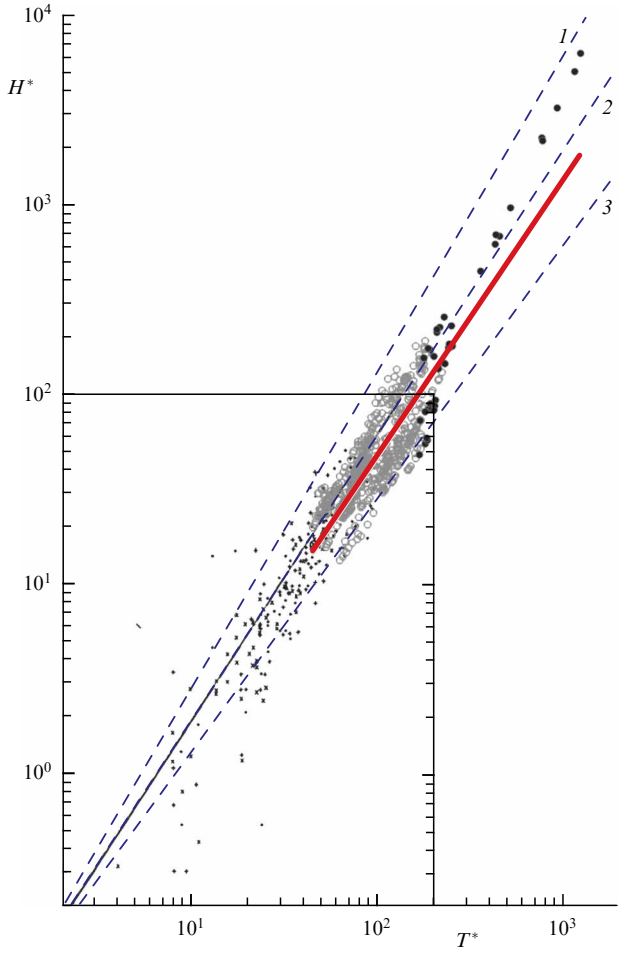

Figure 4. Test of the statistical Toba law based on data for individual waves. *1* — $H^* = 0.062T^{*(3/2)}$, *2* — $H^* = 0.062T^{*(5/3)}$, *3* — $H^* = 0.062\times T^{*(4/3)}$. Black crosses correspond to the results of [10]. Gray and black circles are data obtained on the Gorky Reservoir (gray circles, $\Omega = 1.5-3.5$, black circles, $\Omega = 0.3-0.8$), solid red line is the approximation $H^* = 0.062T^{*(1.448\pm0.003)}$ (see [33] for details).

have continued, in particular, the dependences [31]

$$\frac{Uf_r}{g} = AF^{-\alpha}\,, \quad \frac{g^2\varepsilon}{U^4} = BF^{\beta}\,, \quad \varepsilon = \frac{h_r^2}{16}\,, \tag{23}$$

where h_r is the so-called significant wave height, which is the measure of wave kinetic energy.

Measurements give the exponents α in the range from 0.23 to 0.33, and β in the range from 0.7 to 1.0. These exponents are lower when the water is colder than the air. When the water is warmer, convection develops in the water (and air). It facilitates the transfer of wind momentum and energy to the water. Overall, the process is consistent with ANK34, so that $3\alpha \approx \beta$. In the longest complex measurements [32], $\alpha = 0.33$ and $\beta = 1.0$. Reference [33] compiled numerous measurements of the Toba law $h^2 \sim T^3$, shown in Fig. 4, where the dashed contour lines correspond to the spectral slopes calculated in [34], which differ by $\pm 1/3$ from the basic exponent of -4, the bold line corresponds to $-13/3$ for young waves with $\Omega > 2$ and to $-11/3$ for waves with ages $1.2 > \Omega > 0.83$, and in the gap the exponent is -4, corresponding to waves that are not yet old but already developed (earlier, the age was associated with the inverse quantity).

The wave age influences both the wave spectrum and the dispersion of contaminants over the water surface. The sea wave characteristics which were estimated and tested here affect both the eddy diffusion coefficient, which is slightly reduced, and the pollution area (see [5, 43]), and since the frequency spectrum and the dispersion equation are different here, the exponent in the evolution of the polluted area with time is modified [5].

5. Probability distribution of cloud fields

Statistics on the sizes of cloud fields is the clearest natural manifestation of the Kolmogorov–Obukhov turbulence theory proposed in 1941. This became clear after the detailed analysis of the global cloudiness patterns provided by the special US spacecraft mission CloudSat [35]. The spectra of the horizontal lines $n(L)$ of the lengths of individual clouds and cloudless intervals are shown in Fig. 5. These lengths are approximated as $n(L) = L^{-\beta}\exp[-(L/L_*)^2]$, where $\beta = -1.66 \pm 0.00...$ and $L_* = 1850$ km. A cloud consists of droplets formed from condensed water vapor for a particular combination of humidity and temperature. Both quantities are considered to be passive scalars transported by velocity fluctuations [3].

Slight differences in the spectra for clouds and blue sky regions can be attributed to the ambiguity in defining the boundaries of the experimental regions in the sky. Exactly the same conclusions have also been drawn for the shape of noctilucent clouds — ice particles at an altitude of 80–90 km [36]. So the results for different types of clouds are again the direct consequences of ANK34.

About a half a century ago, Benoit Mandelbrot [37] introduced the concept of a fractal, a power-law statistical relationship between two random quantities. For the characteristics of clouds, it was proposed in [38] to use the relationship between their area $A = R^2 = BP^{\alpha}$ and perimeter $P = CR^{\beta}$. Forty years ago, it was found that $\beta = 1.35$. In the same paper, it was noted that this value is close to $4/3$ (the difference is only $1/60$ [39]). Later, $\beta = 1.35$ was also found for noctilucent clouds [36] and in a number of numerical simulations (see [39]). The explanation for $4/3$ was given in [39]. It is easy to see that from the relation between the area A and its perimeter P it follows that

$$\frac{\alpha\beta}{2} = 1\,, \tag{24}$$

$$BC^{\alpha} = 1\,, \tag{25}$$

$$C = B^{-1/\alpha}\,, \tag{26}$$

and if $\beta = 4/3$, then $\alpha = 3/2$, $C = 0.15^{-2/3} = 3.7\ \text{km}^{-1/3}$.

Unfortunately, the authors of many regression analyses do not give estimates of the uncertainty in the exponents like α and β, even with the standard 95% precision. To estimate their error bounds, in [39], we digitized 76 points of Fig. 1 from [38] and found that $\beta = 1.35 \pm 0.02$. The quantities B and C show an arithmetic pre-fractal relation, which is rarely mentioned in studies dealing with fractal analyses, although it carries some useful information.

Reference [39] proposes a theoretical derivation of $\beta = 4/3$ based on the similarity theory and dimensional analysis and using the results of ANK34. Unfortunately, an expression for line elongation in a turbulent flow based on first principles has not yet been proposed (see [3]).

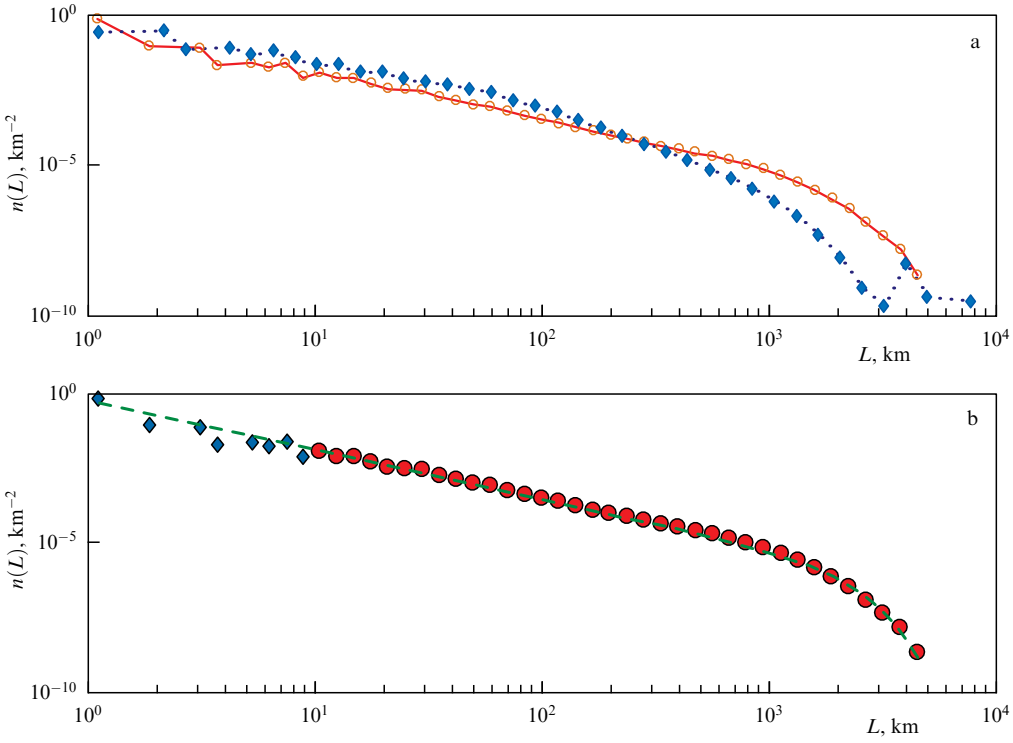

Figure 5. Distributions of horizontal lines $n(L)$ for clouds and cloudless intervals given, respectively, by circles and blue rhombi (a); (b) green line $n(L) = L^{-\beta}\exp\left[-(L/L_*)^2\right]$, where $\beta = 1.66 \pm 0.00$ and $L_* = 1850$ km.

From a dimensional consideration, [39] suggests that the length varies with time as $l_P(t) = [K_1(l,t)\,t]^{1/2}$ and that the length $l_A = [A(t)]^{1/2}$ grows with time according to a parabolic law, and the perimeter $P(t)$ grows with the time $\tau = (l^2/\varepsilon)^{1/3}$, but with $K_1(t)$, i.e., because of turbulence. We can further find the ratio $K_1(t)/K_2$ without concentrating on their individual values. The ratio of the perimeter to the mean radius is the similarity parameter

$$\Pi = \frac{P}{\sqrt{A}} = \frac{B^{-1/\alpha}A^{1/\alpha}}{\sqrt{A}} = \left(\frac{K_1\tau}{K_2 t_2}\right)^{1/2} = \left[\left(\frac{a(R^2/\varepsilon)^{1/3}}{t_2}\right)\right]^{1/2}, \tag{27}$$

where $a = K_1/K_2$ is the ratio of the diffusion coefficients for the perimeter and area. Using $\alpha = 3/2$ and the above relationships, taking into account the pre-fractal values of B and C according to the results of [38], we find with 95% significance

$$\Pi = 3.54A^{1/6} = CR^{1/3}, \tag{28}$$

which illustrates the proximity of the exponent β to 4/3. The similarity parameter $\Pi > 1$ is the ratio of the cloud perimeter to the mean cloud size. To obtain the dissipation rate ε, we use the result of [40] that the kinetic energy generation rate in the atmosphere is 2.3 W m^{-2}. With the mass of the atmospheric column $M = 10^4$ kg m^{-2}, we obtain $\varepsilon^{-1/6} = 40.4\,\mathrm{s}^{-1/2}\,\mathrm{km}^{-1/3}$. Then, using (27), we obtain for the similarity parameter Π values from 5.4 to 37.2 for the areas from 10 to 10^6 km^2, averaged over the globe. We stress that the main hypothesis of A N Kolmogorov consists in the Markov character of the forces, i.e., the accelerations acting in the system, and the evolution of the probability density $p(t, u_i, x_i)$ for the 6-dimensional vector written in the form of the Fokker–Planck–Kolmogorov equation corresponds to ANK34.

6. Hurricanes and physical analogs of similar vortices

These formations also follow the laws of ANK34, but for a given basic rotation period and given lower boundary conditions at the interface between the ocean and atmosphere, which are not in thermodynamic equilibrium. The 1990s were proclaimed by the UN as the International Decade for Natural Disaster Reduction. The activities of this decade were guided by the International Scientific Committee chaired by a distinguished British scientist, a member of the academies of several leading countries, including our own, Sir James Lighthill. In 1995, at one of the committee meetings, he said that we still do not understand why the energy of a hurricane can reach the level of the explosive energy of many thousands of H-bombs. This is clarified in Section 1 of the present paper on the background of ANK34, but in 1997 I obtained formula (13) based on the ideas of similarity and dimensional analysis, having estimated separately the speed and size of a hurricane.

The Coriolis force varies with latitude, and for the latitude $\theta = 20^\circ$ $l_C = 5 \times 10^{-5}$ s^{-1}, the heat flux from water together with the latent heat of condensation is estimated to be 1 kW m^{-2}, which gives the buoyancy flux $b \approx 0.03$ m^2 s^{-3}. Hurricanes are also observed over polar seas, when cold air with temperatures $T \leqslant -30^\circ$C from the latitudes covered by sea ice intrudes into areas with water temperature $T \approx 0^\circ$. References [5, 42, 43] give nomograms that specify *necessary* conditions for the occurrence of intense vortices. Their construction takes into account the conditions of water evaporation and subsequent heat release due to water vapor condensation, as well as the change in the thermodynamic parameters that depends on temperature. Since the vortex area is inversely proportional to l_C^3, polar hurricanes, called

mesocyclones, are typically several times smaller than their tropical counterparts, as is observed in nature [5, 16]. The exchange of momentum, heat, and moisture in this case is routinely described by the so-called bulk formulas. These semi-empirical formulas all include proportionality to U_{10}, i.e., a wind speed at 10 m in height. Since ANK34 allows the squared velocity to be estimated from meteorological data, this provides an additional estimate of hurricane size. Tropical hurricanes develop within half a day, polar hurricanes, within several hours, which was taken into account in the construction of the nomograms for the necessary condition of vortex development, while the stratification of the atmosphere, important for obtaining *sufficient* conditions, was taken into account only in the mean. The insufficient accuracy of satellite measurements of the vertical structure of the atmosphere will delay the development of numerical forecasts based on satellite data for a long time (if not forever). However, if such a vortex is already present, the numerical weather forecast models can predict its motion with ever increasing accuracy.

Spiral vortices on the surface of seas and oceans, which again occur when the atmosphere is colder and are seen when sea waves are weak [44], are described analogously. These spiral vortices are not observed in the $\pm 5^\circ$ equatorial band. When water is cooled from the surface, convection that develops in the water is characterized by the flux of buoyancy b which is five orders of magnitude smaller than in hurricanes, since the material parameters for water differ substantially from those for air. This leads to vortices with diameters of several kilometers and velocities of ~ 5 cm s^{-1} [43, 45].

During the Second World War, massive fires accompanied the bombing of Hamburg, Dresden, and Hiroshima. Convection of hot air from large fire areas causes lateral inflow of surrounding air masses, which concentrates angular momentum and creates a fire tornado. Simulations [46] show that, after the onset of a model fire, the emerging cyclonic vortex develops hurricane-like velocities up to 70 m s^{-1} (in accordance with the laws of ANK34!) within several hours.

The similarity of large-scale processes in nature is obvious and they provide inspiration to study them in more detail.

7. Statistical structure of the relief on the surface of celestial bodies

Space research has uncovered many new laws for which there was no physical understanding for decades. The first of these is the Kaula rule [47, 48]. It was found that fluctuations in gravitational force, and then of the relief, expanded in a series in spherical harmonics, starting from $n \geqslant 4$ decay as n^{-2}. Later, the same was established for the Moon, Mars, and Venus, and also for smaller bodies (see [5, 50, 51]). An explanation and the sense of this law were given only in 2019 [5, 50, 51] and are based on the ANK34 rules or, even simpler, on the standard Fokker–Planck equation for the probability density of the relief field $p(y, h)$, where y is the meridional coordinate and h is the vertical one.

The standard form of the Fokker–Planck equation is

$$\frac{\partial p}{\partial t} = D\,\frac{\partial^2 p}{\partial h^2}\,, \quad p = p\big(h(t), t\big)\,, \tag{29}$$

where $h(t)$ is the random altimeter record. For a known flight speed u, the recorded time is transformed into the horizontal coordinate $y = ut$, and then

$$\frac{\partial p}{\partial y} = D_1\,\frac{\partial^2 p}{\partial h^2}\,, \quad D_1 = \frac{D}{u}\,, \tag{30}$$

whose second moment has the form $\langle h^2(y)\rangle = 2(D/u)y$, and this structure function has a spectrum

$$S(k) = \frac{D}{2\pi}\,k^{-2}\,, \quad k = \frac{2\pi}{\lambda_y}\,, \tag{31}$$

where λ_y is the horizontal wavelength of the random relief. This equation is valid for small regions $2 < y < 60$ km [5, 48]. Based on measurements in the state of Oregon for 24 flights in different directions over mountainous, hilly, and flat regions, $S(k) \sim k^{-n}$, where $n = 2.03 \pm 0.04$.

Performing all the necessary manipulations with spherical harmonics [50, 51], we find for the vertical component of the relief

$$S_n = \frac{4\pi r D_1}{n(n+1)}\,, \tag{32}$$

where r is the radius of the celestial body, i.e., the harmonics decay slightly faster than n^{-2}. Book [48] presents 180 spherical harmonics for Earth and 60 for Venus in logarithmic scales. Processing the harmonics in the first case gave $D_1 = 1.3 \pm 0.3$ m, and in the second, $D_1 = 0.2 \pm 0.03$ m with an accuracy of about 20%. The Venusian atmosphere is 65 times denser, so that the erosion processes on it are more intense than on Earth, and the relief is an order of magnitude less pronounced.

Other surface features, modified by other erosion processes, defined by the climate, first and foremost by precipitation, evaporation, soil structure, etc., are linked to the spatial relief spectrum proportional to k^{-2}. Therefore, the cumulative distribution of the number of rivers over length l behaves as $N(\geqslant l) \sim l^{-n}$ with $n = 1.9$, and for the distribution of lakes over an area S, we have $N(\geqslant S) \propto S^{-n}$ with $n = 0.95$ (see [4, 46]). The equality of the exponents in the cumulative distributions of river length and mean linear lake size clearly points to the role of relief. A small deviation in n from 1 or 2 is indicative of the role of large-scale erosion processes, which shape the relief in a purely random Markov manner.

The celestial bodies are finite spheres, and their spectral harmonics are discrete. A corresponding analysis using the associated Legendre polynomials was carried out in [49–51]. The derivative of the relief over the angle, i.e., the slope $g\cos\theta$, is a random Markov variable. Water flows over the slope, boulders roll down it, the slope resists wind action, i.e., it is a factor forming the relief. Performing the necessary operations, we find the expression for the spherical harmonic in the form [50]

$$S_n = \frac{\alpha^2}{n(n+1)}\,, \qquad E_n = 2\pi r^2 \sum_{n=1}^{\infty} S_n\,, \tag{33}$$

where α^2 is the mean square of the random angle.

8. Size distribution of water reservoirs and the damage caused by floods

When I was the director of the Institute of Atmospheric Physics (1990–2008), my scientific thoughts were far from the subject of hydrology. However, in 1998, I saw a graph

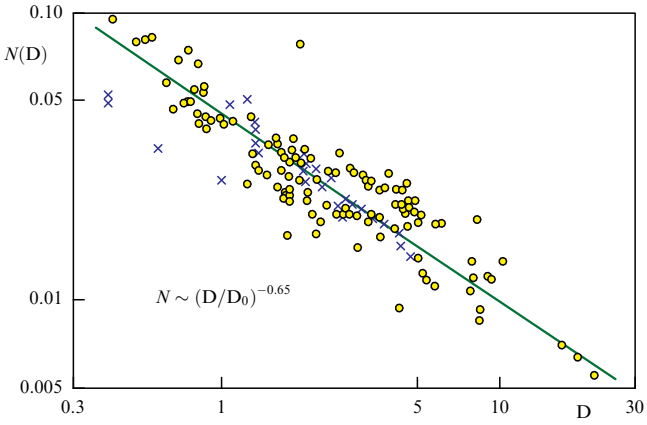

Figure 6. Cumulative distribution of the number of floods versus their damage [53].

showing the value of the damage D caused floods (Fig. 6):

$$N(\geqslant \mathrm{D}) \sim \mathrm{D}^{-n}\,, \qquad n = 0.65\,,$$

without the limits on n, but visually they were ± 0.03. For about 20 years, I kept this in mind, noting that 0.65 is close to 2/3. After 2008, I continued as a professor of climate theory at Lomonosov Moscow State University (MSU) and the Moscow Institute for Physics and Technology (MIPT) and started to write a book [52] on these issues.

The damage is estimated by the flooded area, which depends on the relief, and the random quantity is the volume of precipitation,

$$V = p\tau S\,, \tag{34}$$

where p is the mean precipitation rate during the time τ over the river catchment area S. In this case, our formula (34) shows that the cumulative distribution of precipitation over the volume (see Section 1)

$$N(\geqslant V) \sim AV^{-1}\,,$$

where A is a quantity with the dimension V/T. We assume that the damage $\mathrm{D} = \alpha V$ is proportional to the volume of precipitation, where $[\alpha] = \mathrm{D}V^{-1}$, and D is the dimension of the damage, for example, in monetary units. The flooded area $S_y = h\beta^{-1}L$, where $h = h(V)$ is the mean flood depth, β the mean angle of the river valley side slope, and $L \sim h/\beta_1$ is the length of the flooded valley, where β_1 is the slope coefficient of the river discharge.

Specific damage per unit area will be $y = \alpha_1 h$, where $[\alpha_1] = \mathrm{D}L^{-3}$. The volume of water flooding the territory will be

$$V = hS_y = \frac{yS_y}{\alpha_1} = \frac{\mathrm{D}}{\alpha_1}\,,$$

and at the end $V \sim hS_y = \alpha_1 h^3/\beta\beta_1$. The area and the damage are determined by the geomorphological parameter $\beta\beta_1$, which depends on the concrete conditions and serves as a natural similarity parameter defined by external conditions. This parameter

$$\Pi = (\beta\beta_1)^{-1/3} = h^{-1}\left(\frac{\mathrm{D}}{\alpha_1}\right)^{1/3}. \tag{35}$$

We rewrite the empirical considerations in a general form,

$$N(\geqslant \mathrm{D}) = c(\Pi)\alpha \mathrm{D}^{-1}\,, \tag{36}$$

where we allow the numerical coefficient c to depend on the similarity parameter. Leaving only the first linear term in the expansion $c(\Pi) \sim \Pi$, we find $\Pi(\mathrm{D}) \sim \mathrm{D}^{1/3}$, in good agreement with empirical expression (36).

This derivation is presented with additional details in [54]. In the same reference, we also presented data on statistics of 'turbid mushrooms,' areas of the sea surface occupied by turbid plumes from river discharges: the areas of these mushrooms are $P \sim A^b$, $b = 0.6-0.7$, and their number as a function of area is distributed as $N(\geqslant P) \sim P^{-\beta}$, $\beta = 1.02 \pm 0.03$. Thus, all these results are governed by the relationships between the catchment areas A with the flooded areas P and the volume V of precipitation over them. It should be recalled that $[S] = [V]^{2/3}$ by dimension, i.e., a lower layer of precipitation is essential.

9. Discussions of results and conclusions on the role of ANK34

The reader is reminded that the ANK34 theory describes *random motions* and not *random walks*, as the ordinary Fokker–Planck equation does. We list the main points of ANK34 for the Markov character of the accelerations:

(1) The proportionality of the mean velocity squared, i.e., the energy per unit mass, to the time in random processes. L D Landau was the first to mention this relation in the first edition of the *Mechanics of Continuous Media* in 1944. The statistics of the set of random events follows from here in the form of cumulative distributions $N(\geqslant E) = C\varepsilon/E$, where ε is the measure of process excitation, and C is a dimensionless coefficient which may depend on the dimensionless similarity parameters acting in the system [7]. Such is the distribution of cities by population size, stones on the surface of Mars by weight, or the relief spectrum of celestial bodies (see Section 7 and [5]). Such is the occurrence law for earthquakes with two intervals in their spectrum (see Section 3 and [5]).

(2) The proportionality of the mean square of the distance between random events to the cube of time, i.e., the proportionality of the structure function to t^3, and the associated frequency spectrum to ω^{-4}, which corresponds to most sea waves and the Toba relation [10] between the square of wave peak height and the period $h^2 \sim T^3$, the latter simply being relationship (3).

(3) For terrestrial hurricanes, this explains why their energy is on the order of the explosive energy of thousands of megaton bombs. Formula (12) contains the product of the first and second moments of ANK34 multiplied by the air mass with the time replaced by an expression based on the Coriolis parameter $l_C = (4\pi/T)\sin\theta$, where θ is the latitude. Since the result includes l_C^{-4}, polar hurricanes (mesocyclones) are several times smaller than tropical ones.

(4) The cumulative distribution of objects over areas has the dimension of inverse time, so, according to (3), $N(\geqslant S) = C(\varepsilon/S)^{-1/3}$, and the lithospheric plates are empirically distributed with the exponent 0.33 [12]. Spiral galaxies are distributed over masses in the same way [5], which can be understood under the assumption that their masses are proportional to their areas.

(5) Systems can have their own similarity parameters, which can modify the self-similarity regimes of the processes

under study; this should always be kept in mind [7], and here the notion of intermediate asymptotic forms emerges [7–9].

(6) The existence of the self-similar form of equation (1), the basis of ANK34, paves the way for its use in the description of other probabilistic processes.

All this illustrates the idea that, on a large scale, nature strives to configure itself according to general laws. The book [5] contains two epigraphs. The first one is by Gibbs: "The goal of science is to find the point of view from which the problem can be solved in the simplest and most natural way." It can be argued that ANK34 extended by the similarity theory and dimensional analysis can solve a wide range of questions and in this sense corresponds to Gibbs's goal. The second epigraph belongs to A N Kolmogorov (according to [7]) and was formulated about half a century ago: "Randomness is a necessary, if not the most important, element of nature, and yet it possesses a certain order which leads to concrete, often stable structures. Stability is limited in time and space, depending on concrete conditions." This order manifests itself in the asymptotic forms of the moments of the distributions. Thus, ANK34, with additions from the similarity theory, illustrates both epigraphs.

An addition to the proofs

The same methods as above can be used to calculate the forcing of tornados and storms and their destructive strength. Reference [55] uses data for 164 vortices registered and quantitatively described in Russia for the period 2001–2021. The description gives their linear size near the surface $2R$ in meters. Those vortices with a vertical axis are cylindrically symmetric, so knowing their diameter gives the area $S = \pi R^2$. Their velocities are estimated by the Fujita index, $F0, \ldots, F4$, which is related to the velocity ranges of 18–32, ..., 93–116 m s^{-1}. Mean values are taken for the velocities. Then, to estimate the forcing, $\varepsilon = \bar{u}^2/t = \bar{u}^3/S^{1/2}$, where $t = (\bar{u}^2/S)^{1/2}$. The destruction in rural areas takes place roughly in the lower 10 m (up to 30 m in forests), and then the vortex energy in the lower 10 m of the atmosphere for an area of 100 m^2 is in the limits from 4×10^7 to 1.1×10^{11} J, and the energy needed to damage a house with a volume of 10^3 m^3 will be from 10 kg to 26.4 t in units of TNT equivalent, which is now not far from nuclear artillery.

Acknowledgments. Finally, I would like to express my gratitude to my teachers and colleagues who taught me how to work and discuss the results. First and foremost, I am grateful to the academician A M Obukhov (director of the Institute of Atmospheric Physics founded by him in 1956 and now named after him), who admitted me to his institute on 1 February 1958, saying that he would like to see in me a geophysicist with a broad profile. I am also grateful to my senior colleagues A S Monin, A M Yaglom, and G I Barenblatt, who taught me how to do science and analyze results. I am indebted to dozens of other colleagues in Russia and in many other countries.

References

1. Kolmogoroff A *Ann. Math.* **35** 116 (1934) *
2. Obukhov A M, in *Advances in Geophysics* Vol. 6 (Eds H E Landsberg, Van Mieghem) (New York: Academic Press, 1959) p. 113, https://doi.org/10.1016/S0065-2687(08)60098-9
3. Monin A S, Yaglom A M *Statistical Fluid Mechanics*: *Mechanics of Turbulence* Vol. 2 (Cambridge, MA: MIT Press, 1975); Translated from Russian: *Statisticheskaya Gidromekhanika. Mekhanika Turbulentnosti* Vol. 2 (Moscow: Nauka, 1967)
4. Golitsyn G S *Russ. Meteorol. Hydrol.* **43** (3) 135 (2018); *Meteorol. Gidrol.* (3) 5 (2018)
5. Golitsyn G S *Veroyatnostnye Struktury Makromira*: *Zemletryaseniya, Uragany, Navodneniya...* (Probabilistic Structures of Macroworld: Earthquakes, Hurricanes, Floods...) (Moscow: Fizmatlit, 2022)
6. Gledzer E B, Golitsyn G S *Dokl. Phys.* **55** (8) 369 (2010); *Dokl. Ross. Akad. Nauk* **433** (4) 466 (2010)
7. Barenblatt G I *Scaling* (Cambridge: Cambridge Univ. Press, 2003) https://doi.org/10.1017/CBO9780511814921; Barenblatt G I *Avtomodel'nye Yavleniya — Analiz Razmernostei i Skeiling* (Self-similar Phenomena — Dimensional and Scaling Analysis) (Dolgoprudny: Intellekt, 2009)
8. Barenblatt G I, Zel'dovich Ya B *Russ. Math. Surv.* **26** (2) 45 (1971); *Usp. Matem. Nauk* **26** (2) 115 (1971)
9. Barenblatt G I, Zeldovich Ya B *Annu. Rev. Fluid Mech.* **4** 285 (1972)
10. Toba Y *J. Phys. Oceanogr.* **8** 494 (1978)
11. Toba Y *J. Oceanogr. Soc. Jpn.* **29** (3) 209 (1973)
12. Bird P *Geochem. Geophys. Geosyst.* **4** (3) 1027 (2003)
13. Golitsyn G S *Russ. J. Earth Sci.* **17** ES5001 (2017) http://dx.doi.org/10.2205/2017ES000607
14. Emanuel K A *Annu. Rev. Earth Planet Sci.* **31** 75 (2003)
15. Golitsyn G S *Dokl. Earth Sci.* **354** (4) 633 (1997); *Dokl. Ross. Akad. Nauk* **354** (4) 535 (1997)
16. Rasmussen E A, Turner J (Eds) *Polar Lows*: *Mesoscale Weather Systems in Polar Regions* (Cambridge: Cambridge Univ. Press, 2003)
17. Golitsyn G S *Dokl. Earth Sci.* **346** (1) 166 (1996); *Dokl. Ross. Akad. Nauk* **346** (4) 536 (1996)
18. Kasahara K *Mechanics of Earthquakes* (Cambridge: Cambridge Univ. Press, 1981)
19. Schubert G, Turcotte D L, Olson P *Mantle Convection in the Earth and Planets* (Cambridge: Cambridge Univ. Press, 2001) https://doi.org/10.1017/CBO9780511612879
20. Golitsyn G S *Comput. Seismol.* (32) 138 (2001)
21. Smirnov V B, Ispolinova S I *Dokl. Ross. Akad. Nauk* **342** (6) 809 (1995)
22. Volant P, Grasso J-R *J. Geophys. Res.* **99** 21879 (1994)
23. Nikolaev A V, Galkin I N (Exec. Eds) *Navedennaya Seismichnost'*: *Gosudarstvennaya Nauchno-Tekhnicheskaya Programma Rossii "Global'nye Izmeneniya Prirodnoi Sredy i Klimata"* (Induced Seismicity: State Scientific and Technical Program "Global Changes in the Natural Environment and Climate") (Moscow: Nauka, 1994)
24. Cheng B et al. *Nature* **382** 518 (1996)
25. Golitsyn G S *Astron. Lett.* **24** (6) 716 (1998); *Pis'ma Astron. Zh.* **24** (11–12) 827 (1998)
26. Berezinskii V S et al. *Astrophysics of Cosmic Rays* (Ed. V L Ginzburg) (Amsterdam: North-Holland, 1990); Translated from Russian: *Astrofizika Kosmicheskikh Luchei* (Ed. V L Ginzburg) 2nd ed. (Moscow: Fizmatlit, 1990)
27. Malkov M A, Diamond P H *Phys. Plasmas* **8** (5) 2401 (2001)
28. Karelin A V et al. *J. Exp. Theor. Phys.* **119** (3) 448 (2014); *Zh. Eksp. Teor. Fiz.* **146** (3) 513 (2014)
29. Golitsyn G S *Astron. Lett.* **31** (7) 446 (2005); *Pis'ma Astron. Zh.* **31** (7) 500 (2005)
30. Golitsyn G S *Phys. Usp.* **51** (7) 723 (2008); *Usp. Fiz. Nauk* **178** (7) 753 (2008)
31. Komen G J et al. *Dynamics and Modelling of Ocean Waves* (Cambridge: Cambridge Univ. Press, 1994)
32. Hasselmann K et al. *Ergänzung Deutsch. Hydrogr. Z. A* **8** (12) 1 (1973)
33. Golitsyn G S, Troitskaya Yu I, Baydakov G A *Izv. Atmos. Ocean. Phys.* **57** (1) 60 (2021); *Izv. Ross. Akad. Nauk Fiz. Atmos. Okeana* **57** (1) 67 (2021)
34. Gagnaire E, Benoit M, Badulin S I *J. Fluid Mech.* **669** 178 (2011)
35. Guillaume A et al. *J. Atmos. Sci.* **75** (7) 2187 (2018)
36. von Savigny C et al. *Geophys. Res. Lett.* **38** (2) L02806 (2011) https://doi.org/10.1029/2010GL045834

* Translation into Russian of A N Kolmogorov's works, see many publications since 1983.

37. Mandelbrot B *Fractals, Form, Chance, and Dimension* (San Francisco: W.H. Freeman and Co., 1977)
38. Lovejoy S *Science* **216** (4542) 185 (1982)
39. Golitsyn G S, Chkhetiani O G, Vazaeva N V *Izv. Atmos. Ocean. Phys.* **58** (6) 645 (2022)
40. Oort A H *Mon. Weather Rev.* **92** (11) 483 (1964)
41. Golitsyn G S *Izv. Atmos. Ocean. Phys.* **44** (5) 537 (2008); *Izv. Ross. Akad. Nauk Fiz. Atmos. Okeana* **44** (5) 579 (2008)
42. Golitsyn G S *Adv. Atmos. Sci.* **26** 585 (2009)
43. Golitsyn G S *Izv. Atmos. Ocean. Phys.* **48** (3) 350 (2012); *Izv. Ross. Akad. Nauk Fiz. Atmos. Okeana* **48** (3) 391 (2012)
44. Munk W et al. *Proc. R. Soc. Lond. A* **456** 1217 (2000)
45. Mityagina M I, Lavrova O Yu *Issled. Zemli Kosmosa* (5) 72 (2009)
46. Andrianov S A et al. *Izv. Atmos. Ocean. Phys.* **39** (1) 1 (2003); *Izv. Ross. Akad. Nauk Fiz. Atmos. Okeana* **39** (1) 3 (2003)
47. Kaula W M *Theory of Satellite Geodesy*; *Applications of Satellites to Geodesy* (Waltham, MA: Blaisdell Publ. Co., 1966)
48. Turcotte D L *Fractals and Chaos in Geology and Geophysics* 2nd ed. (Cambridge: Cambridge Univ. Press, 1997)
49. Rexer M, Hirt C *Surv. Geophys.* **36** (6) 803 (2015)
50. Gledzer E B, Golitsyn G S *Russ. J. Earth Sci.* **19** ES6007 (2019)
51. Gledzer E B, Golitsyn G S *Dokl. Earth Sci.* **485** (Pt. 2) 391 (2019); *Dokl. Ross. Akad. Nauk* **485** (4) 493 (2019)
52. Golitsyn G S *Statistika i Dinamika Prirodnykh Protsessov i Yavlenii* (Statistics and Dynamics of Natural Processes and Phenomena) (Synergetics: from Past to Future, No. 68) (Moscow: Krasand, 2012)
53. Smith K, Ward R *Floods*: *Physical Processes and Human Impacts* (Chichester: Wiley, 1998)
54. Golitsyn G S *Water Resources* **45** (4) 503 (2018); *Vodn. Resursy* **45** (4) 380 (2018)
55. Golitsyn G S, Chernokulsky A V, Vazaeva N V *Dokl. Earth Sci.* **513** (Pt. 1) 1211 (2023) https://doi.org/10.1134/S1028334X23601554; *Dokl. Ross. Akad. Nauk* **513** (1) 134 (2023)